Available online at www.sciencedirect.com
SCIENCE DIRECT®
International Journal of Heat and Fluid Flow 25 (2004) 173–179
International Journal of HEAT AND FLUID FLOW
www.elsevier.com/locate/ijhff

Turbulence production by a steam-driven jet in a water vessel

R.J.E. van Wissen [a], K.R.A.M. Schreel [a], C.W.M. van der Geld [a,*], J. Wieringa [b]

[a] Department of Mechanical Engineering, Division Thermo Fluids Engineering, Eindhoven University of Technology, P.O. Box 513, 5600 MB Eindhoven, The Netherlands
[b] Unilever Research and Development, P.O. Box 114, 3130 AC Vlaardingen, The Netherlands

Abstract

Direct steam injection is an efficient means of heating a volume of liquid. Usually the steam is injected via a nozzle, yielding a strong jet that condenses rapidly and transforms into a self-similar single phase jet. In the experiments reported in this paper, superheated steam is injected, centrally, at the bottom of a vertical, cylindrical water vessel. The resulting jet is turbulent ($Re = 7.9 \times 10^4$–18.1×10^4 with the length scale based on the width of the jet, $r_{1/2}$, and the velocity scale based on the centerline velocity, U_0). Using PIV in a vertical plane through the central axis, instantaneous velocity fields have been measured at a rate of 15 Hz. Near the inlet, the jet is mainly steam that rapidly condenses. Further downstream, the jet is essentially single phase, although some residual air is present as microscopically small bubbles. In the area directly downstream of the steam part, the ratio of $r_{1/2}$ to the vessel radius R (32.5 cm) is about 1/14. The production of turbulent kinetic energy has been quantified for the main process conditions. Its dependencies on temperature, nozzle opening and inlet steam pressure have been determined. This production of energy is related to the stresses exerted on small particles in the mixture, and break-up of particles is discussed.

Keywords: Turbulence production; Jet; Steam condensation; Mixing; Velocity similarity

1. Introduction

When fluid is emitted from a circular or ring-shaped orifice into a larger space, an axisymmetric jet is formed. Jets are important in many unit operations, e.g. those occurring in the combustion, propulsion and process industries. An important application is in mixing, and in this case the enclosure is usually confined or semi-confined, and a recirculating flow is driven and entrained by the jet. A particularly high mixing rate combined with high heat transfer rates is achieved with a superheated steam jet that condenses in a water vessel. Such a jet can, however, damage soft particles in the liquid.

This paper reports results and analysis of experiments performed with a steam jet originating from a circular orifice (with an opening in the shape of a ring) with an outer diameter, d, of 3 cm. The steam condenses rapidly in the center of a cylindrical container having a diameter of 65 cm. The velocity profile in the region above the condensation region is self-similar (Van Wissen et al., submitted), with a small downward velocity near the wall due to recirculation. The jet entrains this recirculation flow, causing the liquid (water) in the vessel to have a nearly homogeneous temperature. Velocity field histories are measured with PIV in the area where the jet is essentially single phase.

A large number of detailed studies concerning single phase jets are known. We will limit ourselves to mentioning the experimental work by Hussein et al. (1994) and Panchapakesan and Lumley (1993), which both used a flat-top velocity profile near the nozzle exit. The reader is referred to these papers for a larger overview of the available literature on single-phase jets. The main focus of these papers has been on the self-similarity of velocity profiles in these jets and their turbulence properties, and in particular the validation of higher order closure models. According to the DNS computations of Boersma et al. (1998), the coefficients of the self-preserving solutions to the axisymmetric jet equations are dependent on the orifice geometry and other initial conditions. The source velocity profile (top-hat, fully developed pipe flow or others) and the source Reynolds

* Corresponding author. Tel.: +31-40-2472923; fax: +31-40-2475399.
E-mail address: c.w.m.v.d.geld@tue.nl (C.W.M. van der Geld).

0142-727X/$ - see front matter © 2003 Elsevier Inc. All rights reserved.
doi:10.1016/j.ijheatfluidflow.2003.11.013

number (*Re*) determine the above-mentioned coefficients, and therefore turbulence properties. For a condensing jet, these parameters are unknown (if they can be defined at all), and a direct measurement is needed.

In mixing applications, it is often desirable to be able to estimate the stresses exerted by the fluid on small-sized particles. At the high Reynolds numbers prevailing in the jet, most particles have a diameter that is at the lower end of the inertial subrange. Ever since the well-known article of Hinze (1956), the break-up of such particles has been related to the turbulent dissipation rate, ϵ. With PIV measurements, the length scales needed to determine ϵ remain unresolved. However, Panchapakesan and Lumley (1993) and Hussein et al. (1994) showed that away from the core of the jet turbulent dissipation is equal to the turbulence production. Turbulence production has therefore been measured for various inlet conditions and bulk temperatures. With the aid of these data, the critical particle size, i.e. the size corresponding to break-up, can be determined.

2. Experimental

2.1. Test rig

The tank (see Fig. 1) has an aluminum base plate, containing holes for filling and draining. The injector nozzle is mounted into this plate. This industrial steam injector is custom manufactured by Südmo. A positioner from Bürkert (TopControl 8630) is used to operate the nozzle. The central part of the nozzle is lifted in order to create a gap through which steam is injected. The maximum opening height of the nozzle is 10 mm and for the remainder of this work the nozzle opening will be indicated by a percentage of this maximum opening (i.e. 30% opening is 3 mm opening). The nozzle opening height is constantly measured and corrected by a PID system. On top of the base plate a Perspex tube (inner diameter 65 cm, height 130 cm) is mounted. This tube contains the working fluid during measurements. Because of its cylindrical shape, secondary flows caused by corners are absent. Optical distortions are compensated by placing the tube inside a second, square glass tank (80×80 cm). The space between the two tanks is filled with water. To reduce light scattering when applying PIV, a black PVC plate has been placed at the back of the tank.

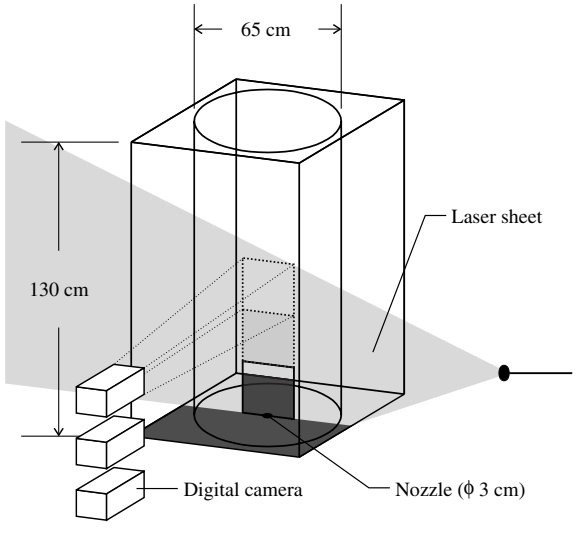

Fig. 1. Sketch of the tank in which the jet is generated and the experimental arrangement. The square shaded area is approximately the field of view used for the strain measurements, and only the lowest camera is used. All three cameras are used for the jet characterization, each with a respective field of view as indicated in the drawing.

If left to itself, the gas–liquid interface at the top is set into violent motion by the jet. The waves that occur will then capture air bubbles in the liquid, which spoil the photos. To reduce this surface motion, a Styrodor grid is used, which floats on the liquid. Due to the strong mixing of the water in the tank by the jet, there are no large temperature gradients in the tank. Therefore only one thermocouple measurement is used to label the PIV measurements.

2.2. Optical technique

A thorough description of particle image velocimetry (PIV) can be found in the work of Raffel et al. (1998) or Westerweel (1993).

The challenge when doing PIV in a two-phase system is mainly posed by the lack of transparency. In a condensing jet this is mostly the case in the (small) region where the jet actually condenses. After this, only small (10–100 μm) bubbles of residual air are present in the jet. Their benefit is that they can be used as tracers together with polyamid seeding in the bulk liquid. Due to the high concentration of the bubbles in the core region of the jet, overexposure may occur. This problem is solved by optimizing the particle concentration and constantly adjusting the diaphragm of the camera. We used 3 g of 20 μm polyamid particles per tank filling (330 l water).

A Nd:YAG laser (Spectra-Physics PIV-200) is used to illuminate the tracer particles, delivering two pulses of 200 mJ at 15 Hz. Through a system of mirrors and lenses a laser sheet is created at the area of interest. The cross correlation camera has a resolution of 1018×1008 pixels with 10 bit digitization (Kodak Megaplus ES-1.0) and is fitted with a 75 mm lens. The timing of laser and cameras is controlled with an SRS DG535 pulse/delay generator. The photos are stored real time to a RAID-0 disk array on a computer with the VideoSavant software package. In order to calibrate the positions, a grid is photographed before each measurement. This positioning of the grid has an accuracy of 0.1 mm.

The PIV analysis is done with software written in-house, based on the work of Westerweel (1993).

2.3. Measurement and analysis

The three main variables to be varied during the experiments are steam pressure (absolute, in MPa), nozzle opening (% of 10 mm) and bulk liquid temperature (°C). Steam pressure and nozzle opening are set before performing the measurements and remain constant during the whole experiment. Liquid temperature is about 15 °C initially (tap water temperature), but this temperature will rise during the experiment due to the heat taken up from the injected steam. All measurements are done at certain values of the liquid temperature rising from 25 to 60 °C with steps of 5 °C. Each set of measurements consists of 100 photos taken at a certain temperature, each series of measurements sets consists of several sets taken at the same inlet pressure and nozzle opening. The interval of 5 °C between the temperature points is chosen large enough to have the time to change the settings on the computer and the camera for the next set of measurements, but small enough to capture temperature effects. The steam pressure is set at 0.3 or 0.4 MPa and the nozzle opening is set at 30% or 50%.

Break up of particles most likely occurs where the shear rates and turbulent production and dissipation are at their maximum. From the measurements it followed that the maximum shear rates and turbulent dissipation occur around the injector nozzle opening. Most of the PIV measurements have therefore been concentrated on the steam jet at a position 5–10 cm above the nozzle, with an imaged area of approximately 7×7 cm in these measurements, see the dark grey bottom square area in Fig. 1.

PIV measurements of multi-phase flows are difficult because of the large amount of bubbles (steam and air) that reflect the laser light. This unavoidably leads to a number of spurious vectors. Because we are interested in shear rates, which are calculated by discrete differentiation of velocity vectors, these vectors need to be removed. We use the median filter proposed by Westerweel (1994). This filter compares a velocity component with the median of its neighbors. If the deviation between a vector and its local median exceeds a certain limit, the vector is replaced by interpolation. The following settings have been used:

- Each velocity component u_i is only compared with its eight closest neighbors.
- The maximum allowed deviation of the velocity component u_i compared to the local median is optimized for each measurement.
- Vectors which exceed this maximum deviation are replaced by an interpolated vector. To calculate this interpolated vector the 24 nearest vectors are used.

Strain rates are calculated using the mid-point difference, but in order to decrease the influence of measurements errors a second order digital filter implementing the analytical derivative of a fitted parabola as proposed by Lanczos (1964) and Hamming (1989) is used:

$$\left.\frac{\partial u}{\partial x}\right|_{x=x_i} \approx \frac{2u_{i+2}+u_{i+1}-u_{i-1}-2u_{i-2}}{5(x_{i+1}-x_{i-1})}. \quad (1)$$

Average values in a turbulent flow field should be by definition ensemble averages. These ensemble averages can be approximated by time averages. A requirement for this is that the total time in which the observations or measurements have been performed is much larger than the macro eddy time scale.

2.4. Measurement errors

Timing errors, calibration errors and errors in the calculation of the displacement vector all may affect the error of the velocity measurements. Timing errors ($<10^{-9}$ s) and calibration errors (0.1 mm absolute, 0.01 mm relative) are negligible in our measurements. Errors in the displacement vectors are due to the cross-correlation procedure, for example: effective averaging of the displacement vector over the interrogation window, false peak detection due to noise, or inaccurate peak detection. The false peak detection and averaging have been minimized by optimization of the measurement process as described above. The accuracy of the peak detection is normally 0.1 pixel, but sometimes displacement vectors tend to take on integer pixel values, commonly referred to as 'peak locking'. In this case it is caused by the fact that the tracer particles (or residual air bubbles) appear as a single pixel on the recordings. Therefore, the position of a peak cannot be determined more accurately than one pixel, the absolute error being ±0.5 pixel. Since this error is unbiased, an average over 50 measurements effectively reduces this.

Errors in pressure settings are approximately 0.01 MPa. The nozzle opening is set with an error of 1%. From extensive thermocouple measurements it follows that the maximum fluctuation in temperature at a point due to the heating up of the liquid during the measurement of a single series of 50 PIV recordings is small. Typical heat-up velocities of the bulk liquid range from 0.1 to 0.2 °C/s, depending on the nozzle opening and the steam pressure. This means that for 50 recordings at 15 recordings per second, the heat-up during the recording is 0.7 °C at maximum. The error of the bulk temperature measurement is estimated a bit pessimistic as 0.5 °C. It is concluded that the velocity field and the production of turbulence are unaffected by the temperature rise in the vessel.

The error in correlations like $\overline{u_r'u_z'}$ is more difficult to assess. We obtained an estimate for this error in the following way. A group of 100 data was split into five groups of 20 data each. The RMS of the variation of

these five averages is taken to be the error estimate (typically 20%). More data would of course yield a better estimate.

3. Results

3.1. Velocity field

The left-hand side of Fig. 2 depicts a schematic of the jet. Steam enters the vessel through the nozzle at $z = 0$, after which it almost fully condenses in a length of 10–15 cm. In this region the jet radius first decreases due to change in density, which is visually observed as a cone shape of steam above the nozzle. After the condensation region the jet becomes a fully developed single-phase water jet. This part of the jet is self-similar (Van Wissen et al., submitted) with a virtual origin (z_0) 10–25 cm upstream of the nozzle. Fig. 2 also comprises a measurement of the vertical component of the velocity over a large area, see Van Wissen et al. (submitted) for more details. This figure indicates a typical boundary of the jet for z larger than 11 cm (for this measurement the data below 11 cm are unreliable). Due to the confinement, there is a small downward velocity near the wall. The time scale of this macro eddy is in the order of 10 s.

For the interpretation of the velocity data, it is important to assess the influence of the temperature gradient inside the container on the jet velocity profile. See Fig. 3 for an impression of the temperature field inside the container. According to Richards and Pitts (1993), buoyancy effects can be neglected for a jet when $z_b < \frac{1}{2}$, with z_b defined as

$$z_b = Fr^{-1/2}\left(\frac{\rho_0}{\rho_\infty}\right)^{-1/4}\frac{z}{d}. \tag{2}$$

The ratio of the densities at the core region (ρ_0) and in the bulk liquid (ρ_∞) is close to one, and the ratio of the height (z) and the nozzle diameter (d) is of the order of 10. The Froude number (Fr) is equal to

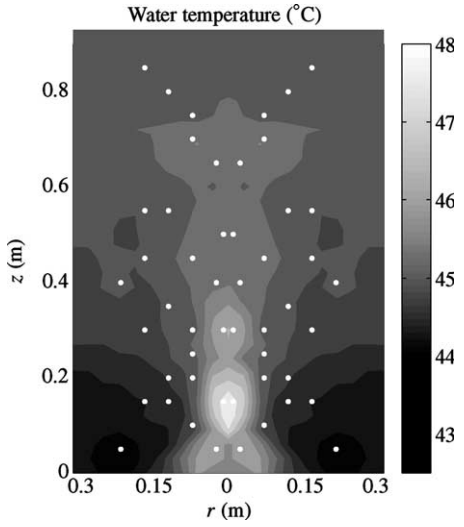

Fig. 3. Instantaneous temperature distribution in the liquid measured with thermocouples. The positions of the thermocouples is indicated with the white dots.

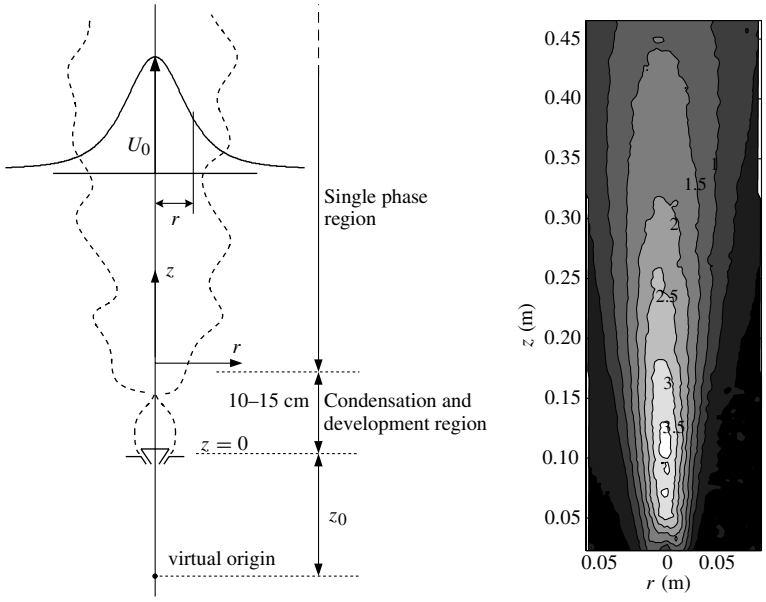

Fig. 2. Left side: schematic representation of the jet, z_0 indicates the distance to the virtual origin. Right side: time-averaged profile of the vertical component of the velocity for an inlet pressure of 0.3 MPa, nozzle opening 30%, and a water temperature of 55 °C. The region below $z = 0.11$ m in this graph is not accurate. These data have been obtained with three cameras simultaneously.

$$Fr = \frac{Re^2}{Gr} \approx 10^{16}. \quad (3)$$

This results in an order of magnitude estimation of $z_b \approx 10^{-7}$. Buoyancy effects can thus be neglected.

3.2. Turbulent production of energy

As will be seen in Section 4, the production of turbulent kinetic energy is important for the description of particle break-up. The production of kinetic energy in the macro scales is given by

$$P_k = -\overline{u_i' u_j'} \frac{\partial \overline{u_i}}{\partial x_j}. \quad (4)$$

There are 50 measurements to average each local gradient of Eq. (4). The same holds for the average velocity and average shear rates (the width of the 95% confidence interval is approximately 15% of the average values). However, the accuracy of the average $\overline{u_i' u_j'}$ on the r.h.s. of Eq. (6) is less (20%). As a consequence, graphs of the mean gradient in horizontal direction of the vertical velocity component and of the turbulent production field are not smooth.

Fig. 4 shows the effects of steam inlet pressure, nozzle opening, and water temperature on the mean strain rate $-\partial u_z/\partial r$. These results show clearly the typical trend. A slight increase with increasing pressure and increasing opening is observed, where the effect of temperature is much more pronounced. Although comparison of the mean strain rate with data of other researchers is not possible, our measurements are validated, to some extent, by the comparison of $\overline{u_z' u_r'}$ data to the ones obtained by Panchapakesan and Lumley (1993), as shown in Fig. 5. Apparently statistics are sufficient to determine the $u_i' u_j'$-correlations needed for the production P_k. A strong effect of temperature is also observed for the turbulent production of kinetic energy (see Fig. 6). Both the shear rate and the turbulent production are negligible outside the jet, as expected. The maximum observed value of the production is about 150 m^2/s^3. That the turbulent production rate depends primarily on the fluid temperature level can be understood in the following way. In single phase jets, the decay of the centerline velocity with increasing distance to the virtual origin, $z - z_0$, is described with a decay parameter B, see for example Pope (2000). The higher B, the higher the dissipation. It is well known that B depends on the velocity profile in the nozzle (Boersma et al., 1998; George, 1989). The velocity profile that actually occurs downstream of the

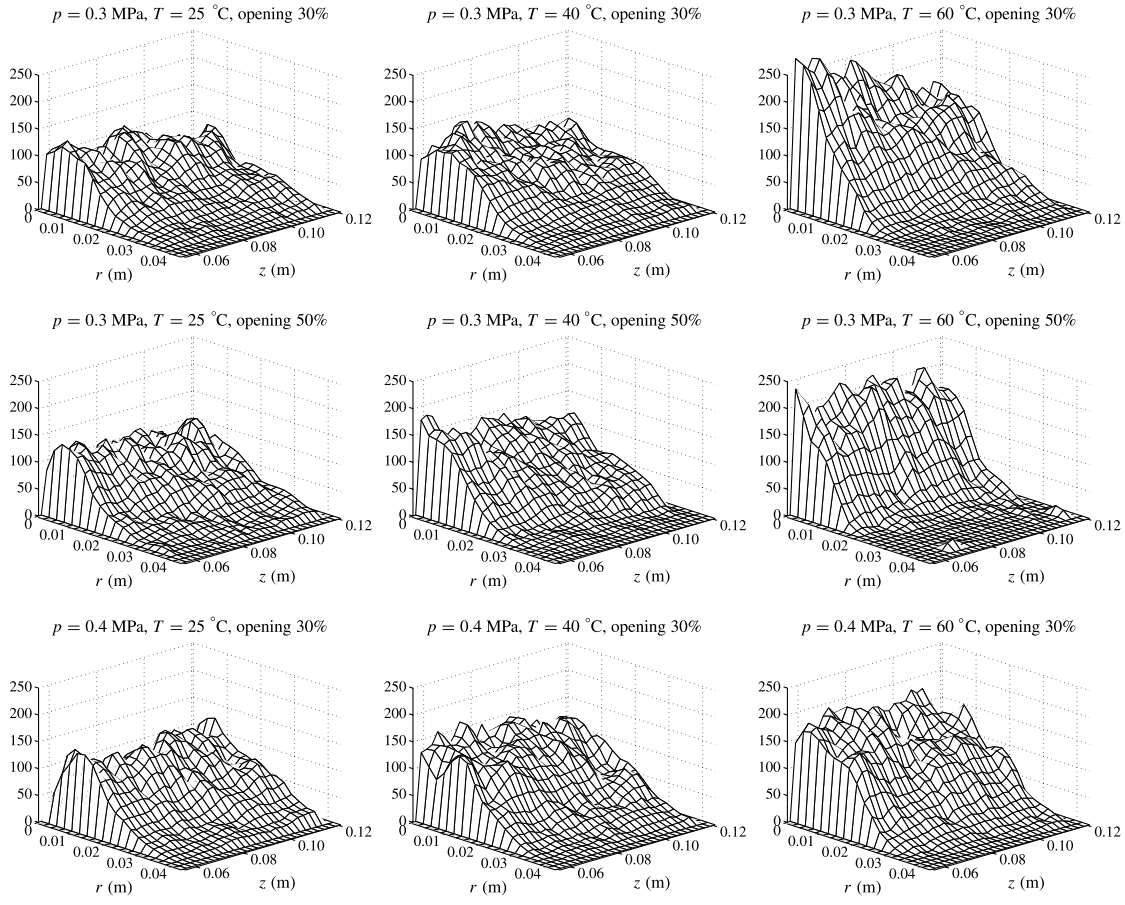

Fig. 4. Mean strain rate ($-\partial u_z/\partial r$ [1/s]) for various bulk water temperatures, nozzle openings, and inlet pressures.

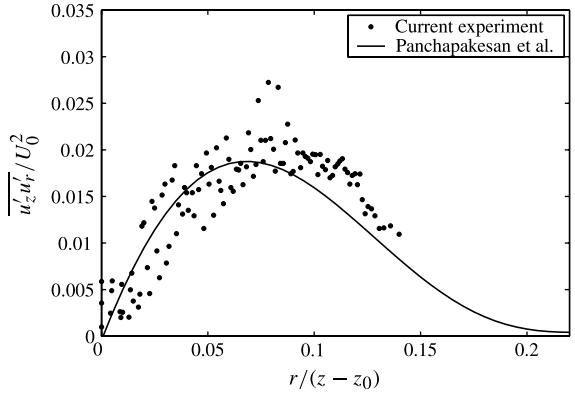

Fig. 5. The correlation between turbulent fluctuations in the radial and axial direction as a function of normalized radial position at a bulk water temperature of 55 °C. Each point represents the median of 10 measurements.

condensing, two-phase region depends on the temperature since Weimer et al. (1973) has shown that the effective width of a two-phase jet increases with increasing temperature. Since the velocity profile depends on temperature, the decay parameter and dissipation depend on temperature as well.

4. Prediction of particle break-up

The two-phase initiated jet studied in this paper yields an efficient way to heat up liquids or mixtures in the process industry. However, in many mixtures in the process industry small particles occur that have a chance of being torn apart if exposed to too high fluid stresses. The limiting particle size in mixing processes is an important parameter. Its predictions are usually based on a lucid article by Hinze (1956). This section presents a summary of a prediction method for particle break-up that utilizes the experimental results presented in Section 3.

The turbulent stresses that may affect a particle can be related to the turbulent structure function (Monin and Yaglom, 1971) over a distance D that equals the particle diameter:

$$\tau = \rho_c \overline{(u'(x,t) - u'(x+D,t))^2}, \tag{5}$$

where $u' = u - \bar{u}$ is the fluctuation of the velocity. If D is in the inertial subrange, the r.h.s. of this equation can be calculated by (see e.g. Batchelor, 1960)

$$\overline{(u'(x,t) - u'(x+D,t))^2} \approx C(\epsilon D)^{2/3}, \tag{6}$$

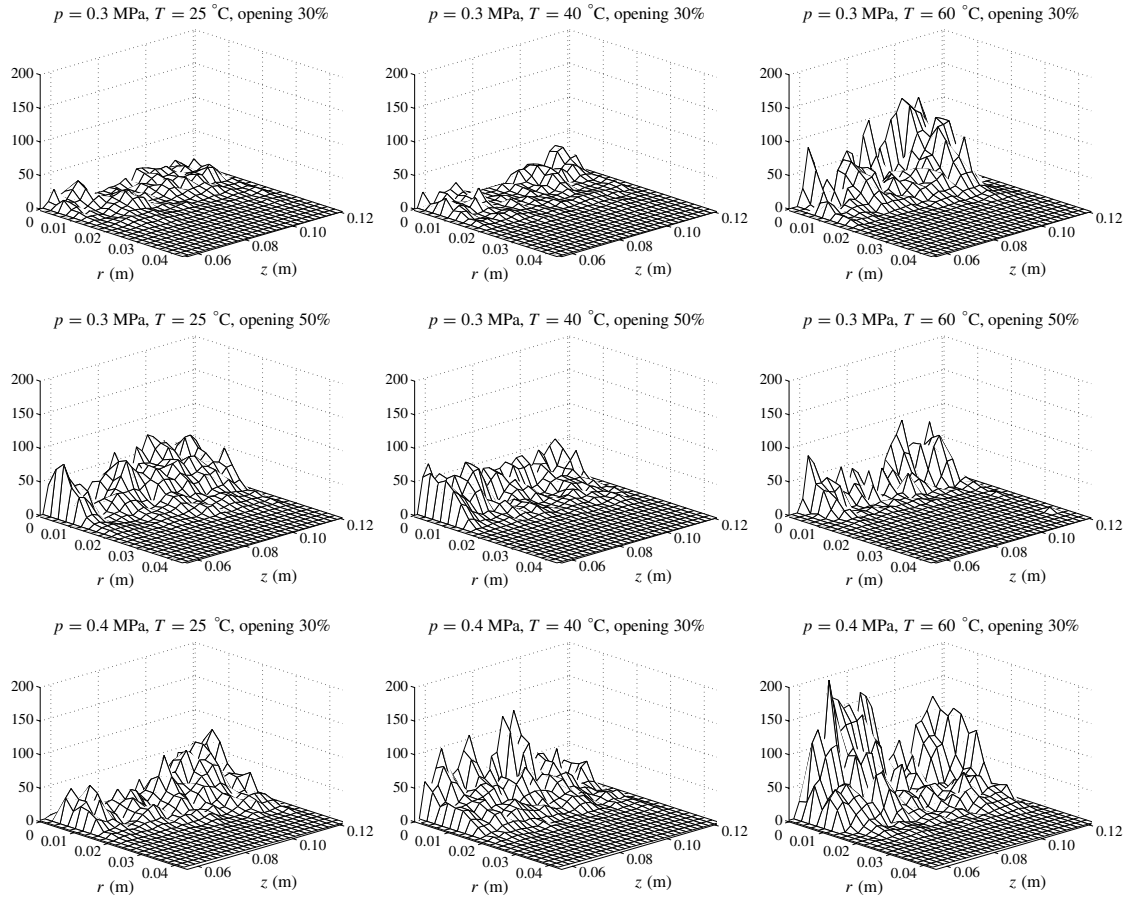

Fig. 6. Turbulence production (P_k [m^2/s^3]) for various bulk water temperatures, nozzle openings, and inlet pressures.

where ϵ is the turbulent dissipation rate per unit mass and C is a constant that has to be determined experimentally. If small, redistributing transport terms are neglected, the turbulent dissipation can be obtained from

$$\epsilon = \nu \sum_i \sum_j \overline{\left(\frac{\partial u_i'}{\partial x_j}\right)^2}, \tag{7}$$

where ν denotes the kinematic viscosity. From experiments it follows that C is approximately 2 for homogeneous turbulence (Batchelor, 1960).

The spatial resolution of the PIV measurements is 1–2 mm. This is much larger than the Kolmogorov length scale, which using $l_\eta = (\nu^3/\epsilon)^{1/4}$ is estimated to be of the order of 10^{-5} m. The turbulent dissipation is therefore estimated from the turbulent production

$$\epsilon \approx P_k. \tag{8}$$

This estimate follows from the equation of transport of kinetic energy by neglecting convective transport terms. This assumption is usually permitted in regions away from the source of turbulence. The turbulent production is obviously extracted from the results presented in Section 3.

From Section 3 it immediately follows that particle break-up is dependent mainly on the mixture temperature in the vessel. For a particle with a diameter of $D = 80$ μm and a liquid temperature of 60 °C, Eqs. (5)–(8) give stresses in the core of the jet of approximately 70 Pa. If the yield stress of a particle would be less, as might be the case for e.g. starch, this particle is expected to break apart.

5. Conclusions

By direct injection of steam through a nozzle in a water vessel, a high heating rate is achieved. In this way a strong jet is obtained, which after condensation is essentially a single-phase (water) jet with a virtual origin much lower than the point of steam injection. This is advantageous for mixing applications with limited space available. For water-based dispersions, however, the turbulence production can be prohibitively large, causing damage to some type of particles.

In this study, experiments are analyzed with respect to the turbulence production of a condensing steam jet. It is found that the production of turbulent kinetic energy mainly depends on the bulk liquid temperature and weakly on inlet steam pressure and nozzle opening. Production increases with increasing temperature, inlet pressure or increasing nozzle opening. From the data presented in Section 3 and the approach summarized in Section 4 the stresses exerted on particles in the fluid can be determined. Break-up would possibly occur in a small flow region close to the nozzle, i.e. the condensing region (see Fig. 2).

The best way to prevent particle break-up while preserving the heating rate is to reduce the inlet velocity of the steam that enters the vessel. With constant inlet mass flow rate of steam this is easily achieved by increasing either the number of nozzles or the diameter of the single nozzle used.

References

Batchelor, G.K., 1960. The Theory of Homogeneous Turbulence. Cambridge University Press, Cambridge.

Boersma, B.J., Brethouwer, G., Nieuwstadt, F.T.M., 1998. A numerical investigation on the effect of the inflow conditions on the self-similar region of a round jet. Physics of Fluids 10, 899–909.

George, W.K., 1989. The self-preservation of turbulent flows and its relation to initial conditions and coherent structures. Advances in Turbulence, 39–72.

Hamming, R.W., 1989. Digital Filters, third ed. Prentice Hall.

Hinze, J.O., 1956. Fundamentals of the hydrodynamic mechanism of splitting in dispersion processes. A.I.Ch.E. Journal 1 (3), 289–295.

Hussein, H.J., Capp, S.P, George, W.K., 1994. Velocity measurements in a high-Reynolds-number, momentum-conserving, axisymmetric, turbulent jet. Journal of Fluid Mechanics 1, 31–75.

Lanczos, C., 1964. Applied Analysis, third printing. Prentice Hall.

Monin, A.S., Yaglom, A.M., 1971. Statistical Fluid Mechanics: Mechanics of Turbulence. MIT Press, Boston.

Panchapakesan, N.R., Lumley, J.L., 1993. Turbulence measurements in axisymmetric jets of air and helium. Part 1. Air jet. Journal of Fluid Mechanics 246, 197–223.

Pope, S.B., 2000. Turbulent Flows. Cambridge University Press.

Raffel, M., Willert, C.E., Kompenhans, J., 1998. Particle Image Velocimetry: A Practical Guide. Springer, Berlin.

Richards, C.D., Pitts, W.M., 1993. Global density effects on the self-preservation behaviour of turbulent free jets. Journal of Fluid Mechanics 254, 417–435.

Van Wissen, R.J.E., Schreel, K.R.A.M., Van der Geld, C.W.E., submitted. PIV measurements of a steam driven, axisymmetric, confined, turbulent water jet.

Weimer, J.C., Faeth, G.M., Olson, D.R., 1973. Penetration of vapor jets submerged in subcooled liquids. A.I.Ch.E. Journal 19 (3), 552–558.

Westerweel, J., 1993. Digital particle image velocimetry—Theory and application. Delft University Press, Delft, The Netherlands.

Westerweel, J., 1994. Efficient detection of spurious vectors in particle image velocimetry data sets. Experiments in Fluids 16, 236–247.